Journal of Sol-Gel Science and Technology (2022) 103:378–385
https://doi.org/10.1007/s10971-022-05844-7

ORIGINAL PAPER: FUNCTIONAL COATINGS, THIN FILMS AND MEMBRANES (INCLUDING DEPOSITION TECHNIQUES)

Characterization of tellurium dioxide thin films obtained through the Pechini method

Murilo Dobri Bataliotti[1] · Francine Bettio Costa[1] · Fernando Brondani Minussi[1] · Eudes Borges Araújo[1] · Nelson Batista de Lima[2] · João Carlos Silos Moraes[1]

Received: 27 March 2022 / Accepted: 10 May 2022 / Published online: 24 May 2022

Abstract

Tellurium dioxide (TeO_2) thin films were deposited on silicon substrates through the Pechini method, after which they were heat treated at different temperatures. The heat treatment temperatures were defined from the thermogravimetry-differential scanning calorimetry (TG-DSC) data of the precursor gel. The effects of the heat treatment on the structural properties were investigated through X-ray diffraction (XRD), atomic force microscopy, and Raman spectroscopy. The TG-DSC data showed four different weight loss steps due to the reduction of telluric acid to tellurium, the removal of the excess ethylene glycol, the decomposition of citric acid, and the degradation of polyester. The XRD and Raman data showed the presence of the γ- and α-TeO_2 phases in the films treated at 400–500 °C. Lattice parameters of the observed crystalline phases were determined by Rietveld refinement, with which it was possible to evaluate the crystallite size and microstrain using the Williamson-Hall method. The heat treatment temperature directly influenced the crystallite size and the surface roughness of the films, which showed similar behaviors with the temperature.

Graphical abstract

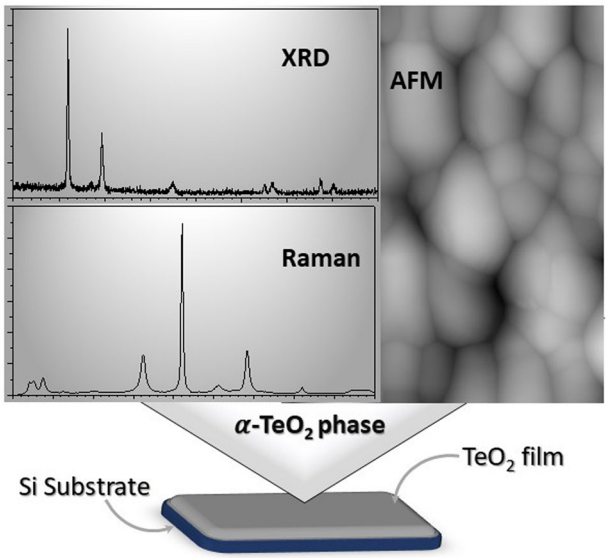

✉ Francine Bettio Costa
franbettiocosta@gmail.com

[1] Department of Physics and Chemistry, São Paulo State University (UNESP), Ilha Solteira, SP, Brazil

[2] Center for Materials Science and Technology, Instituto de Pesquisas Energéticas e Nucleares, São Paulo, Brazil

Keywords Tellurite dioxide · Thin Films · Sol-gel · Rietveld refinement · X-ray diffraction · Atomic force microscopy

Highlights

- Good quality TeO_2 thin films obtained through the Pechini method.
- Phase transformation observed by different techniques.
- Heat treatment temperature versus TeO_2 crystalline phases.
- The coexistence of α- and γ-TeO_2 phases increases films´ strain.

1 Introduction

TeO_2-based materials have been extensively investigated due to their excellent and suitable properties for application in optical devices (e.g., optical switching [1], optical amplifiers [2], optical fiber [3], and temperature sensors [4]) and in γ-ray detectors [5] and gas sensors [6]. Tellurite glasses present high linear refractive index (1.8–2.3), high nonlinear refractive index [7], good optical transmission in the visible and infrared regions (from 0.3 to 6 μm) and low phonon energy (~800 cm^{-1}) [8], while that α and γ-TeO_2 crystalline phases, due to the crystallization of tellurite glasses, present second harmonic generation [9, 10]. However, the practical exploitation of tellurite materials, such as in optical and electronic devices [11, 12], requires that they be in the form of thin films. As an example, in the development of optical-fiber temperature sensors, an alternative method was recently proposed to sensitize the Si fiber tips to temperature by means of the deposition of a tellurium glass film doped with erbium and ytterbium ions [13].

The method commonly used in the preparation of tellurite glasses is melt-quenching. However, this route does not allow to obtain acceptable thin films for application in optical devices. Among the different methods used (thermal evaporation [14], sputtering [15], vacuum deposition [16], pulsed laser deposition [17], and sol-gel [11, 12, 18, 19]), the sol-gel method has been proved to be an alternative route to obtain TeO2 thin films. In addition, this route is attractive to reducing cost and to providing ease of control of the synthesis parameters and high precision in the mixing of different precursors [11, 20].

In the sol-gel method, two tellurium (Te) precursors have been used: Te(IV) alkoxides such as $Te(OCH(CH_3)_2)_4$ and $Te(OC_2H_5)_4$, and telluric acid (H_6TeO_6). The use of Te(IV) alkoxides, despite including low-cost reagents in the process, requires an inert atmosphere and the addition of chemical modifiers to control the hydrolysis reaction [11, 12, 18]. On the other hand, the route that has been used to prepare TeO_2 thin films from telluric acid, in addition to involving several steps, involves the use of expensive and toxic solvents [19, 21].

Given the aforementioned scenario, we propose herein an alternative route in the preparation of thin films of TeO_2: through the Pechini method, using telluric acid as a precursor and low-cost solvents. The structural and morphological properties of the films obtained were investigated as a function of heat treatment at different temperatures.

2 Materials and methods

TeO_2 thin films were prepared using citric acid ($C_6H_8O_7$; Aldrich, 99.5%), telluric acid (H_6TeO_6; Aldrich, 99%), and ethylene glycol ($C_2H_6O_2$, Synth, analytical reagent) as precursor materials.

The precursor solution (polymeric resin) was obtained through the Pechini method, and in its preparation, the molar ratios of the metal ion/citric acid and citric acid/ethylene glycol were fixed at 1:3 and 2:3, respectively. Initially, the citric acid was diluted in deionized water (18.2 MΩcm, 80%, BFilters DEBC-50A-3) under stirring at 70 °C, and then telluric acid was added to form the metal chelates. After 30 min, ethylene glycol was added and the solution was heated to 110 °C and stirred for half an hour to obtain polymeric resin through polyesterization. After this time, heating was suspended and the polymeric resin was kept at rest until it reached room temperature. With this procedure, transparent and stable polymeric resin was obtained.

In the present work (100)-oriented silicon (Si) single crystal plates (Nova Electronic Materials, Ltd) were used as substrates with dimensions of approximately 1 cm^2. In the cleaning procedure, the plates were initially kept in an aqueous solution with neutral detergent at 100 °C for 1 h, and then in hydrochloric acid for 20 s. Subsequently, the surfaces of the plates were rubbed with a soft foam, rinsed with isopropyl alcohol, dried using a spinner, and heated at 100 °C.

TeO_2 thin films were prepared via spin coating. The polymeric resin was dropped onto the Si substrate, which was then rotated at two different spin speeds (1000 and 5000 rpm for 10 and 30 s, respectively). Thereafter, the substrate with the deposited film was dried at 300 °C for 5 min using a hot plate to remove the organic residual. The steps involving deposition, spinning, and drying were repeated 10 times. Finally, the obtained films were heated in

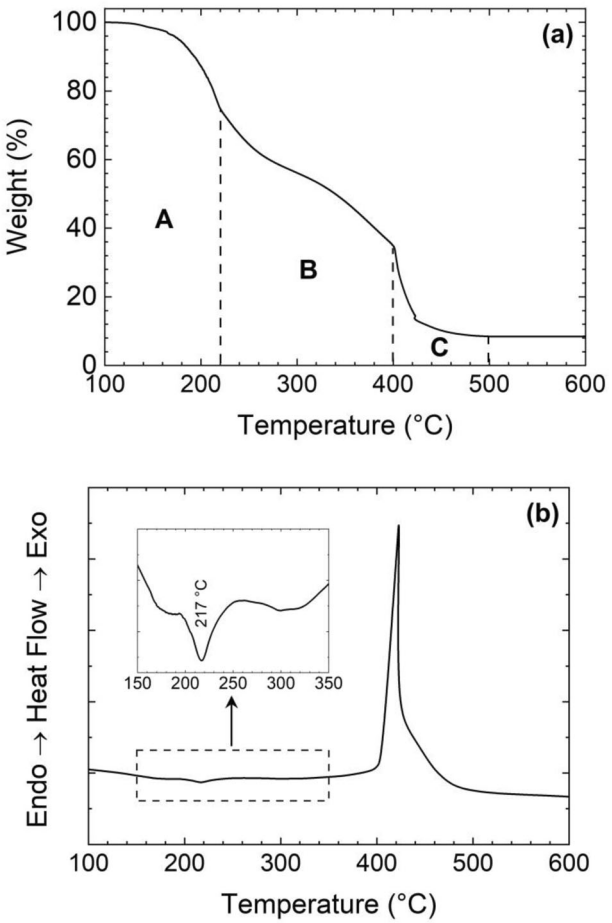

Fig. 1 **a** TG and **b** DSC curves obtained from the precursor gel

an electric furnace for 2 h at different temperatures (350–500 °C).

For thermal analysis, the polymeric resin was heated at 100 °C for 24 h before the performance of thermogravimetry-differential scanning calorimetry (TG-DSC) measurements, resulting in a highly viscous material. The thermal behavior was investigated through TG-DSC analysis using a TA Instruments equipment (model SDT Q600), at 10 °C/min under air atmosphere.

The crystalline phases of the TeO_2 thin films were identified from the X-ray diffraction (XRD) patterns collected on a Shimadzu diffractometer (XRD-6000 model) using CuKα radiation, at room temperature, under 40 kV and 20 mA, in a continuous scan (2°/min), in the Bragg–Bretano configuration. However, the XRD patterns were analyzed through the Rietveld refinement method. The Rietveld refining involves the fitting of a complete experimental diffraction pattern with calculated profiles generated from the structural parameters and background [22] using the GSAS software package [23, 24]. The structural parameter used in this work for each TeO_2 phase was obtained from Inorganic Crystal Structure Database (ICSD) [25] and is better detailed below. The XRD patterns generated by Rietveld refinement were used to estimate the crystallite size and microstrain through the Williamson-Hall method [26]. In addition to the instrumental effects, the Williamson-Hall formula takes into account the effects caused by the crystallite size and lattice strains in the physical broadening of the XRD peaks. Thus, the total broadening can be expressed as

$$\beta_{hkl}\cos\theta = \frac{k\lambda}{D} + 4\varepsilon,\ \sin\theta, \tag{1}$$

where $\beta_{hkl} = \beta_{size} + \beta_{strain}$ is the full width at half maximum (FWHM, in radian) for different diffraction planes, $\beta_{strain} = 4\varepsilon$ tg θ; k is a constant related to the crystalline shape (=0.89); λ is the X-ray wavelength (=0.15406 nm); D is the crystallite size; ε is the strain; and θ is the Bragg angle of the XRD peaks.

The structural properties of the thin TeO_2 films were also investigated via Raman scattering using a micro-Raman equipment (Renishaw model InVia) coupled with a 514 nm laser. The morphology of the thin films was obtained with an atomic force microscope (AFM; Agilent model 5500) in tapping mode. The images obtained were analyzed using the Gwyddion 2.56 software.

3 Results and discussion

Figure 1 shows the TG-DSC thermograms obtained with the precursor gel prepared through the Pechini method. In the TG curve (Fig. 1a), four different weight loss processes can be observed: from 100 °C to 220 °C (A), from 220 °C to 310 °C (B), from 310 °C to 400 °C (C), and from 400 °C to 500 °C (D).

Observed in step A was an endothermic process with a 25% weight loss attributed to the reduction of telluric acid to Te by means of the global redox reaction [27] (eq. [2]), causing the evaporation of methanal, carbon dioxide, and water.

$$C_6H_5O_7^{3-} + H_6TeO_6 + 3H^+ \rightarrow 3CH_2O + 3CO_2 + 4H_2O + Te \tag{2}$$

The global reaction gathers three reactions taking place simultaneously: the oxidation of citrate (Eq. 3); the reduction of telluric acid (Eq. 4); and reduction of tellurium dioxide (Eq. 5). Considering that 100% of the citric and telluric acids in the solution participate in these reactions, the estimated mass loss would be 27%, whose value is very close to that observed in step A of Fig. 1.

$$C_6H_5O_7^{3-} + 2H_2O \rightarrow 3CH_2O + 3CO_2 + 3H^+ + 6e^- \tag{3}$$

$$H_6TeO_6 + 2H^+ + 2e^- \rightarrow TeO_2 + 4H_2O \tag{4}$$

$$TeO_2 + 4H^+ + 4e^- \rightarrow Te + 2H_2O \quad (5)$$

In step B, there was a 40% weight loss attributed to the removal of the excess ethylene glycol [28] ($T_{boiling}$ ~ 197 °C), of the decomposition of citric acid, which resulted in an endothermic peak observed in the DSC thermogram at 217 °C (inset of Fig. 1b) [29], and the removal of organic products from the decomposition of citric acid.

In the last weight loss step (~26%), a variation in the weight loss rate was observed; it was initially faster but later became slower. We believe that there was a competition between the weight loss due to the degradation of polyester and the gain in weight from the oxidation of Te, resulting in an exothermic peak at 423 °C on the DSC curve (Fig. 1b). This exothermic peak was not observed in the DSC thermogram (data not shown here) obtained under a nitrogen atmosphere.

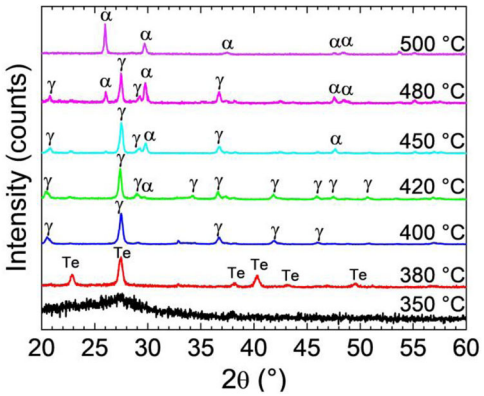

Fig. 2 XRD patterns of the TeO_2 thin films treated at different temperatures

Figure 2 shows the XRD patterns obtained from the TeO_2 thin films treated at different temperatures (350 °C, 380 °C, 420 °C, 450 °C, 480 °C, and 500 °C), which were defined from the DSC data (Fig. 1b). The thin film treated at 350 °C showed an amorphous structure. With heat treatments above 350 °C, it was possible to observe the presence of the metallic Te at 380 °C, and the transformation of the metastable γ-TeO_2 phase to the stable α-TeO_2 phase, which occurred within the 400–500 °C temperature range. The non-observation of metallic Te in the film treated at 400 °C corroborates our initial hypothesis that Te oxidation occurs in the D region of the DSC thermogram. According to the DSC data (Fig. 1b), the exothermic process, attributed to the formation of TeO_2, starts at 400 °C. Therefore, heat treatments at 380–400 °C and the availability of oxygen in the environment favored the formation of TeO_2 from metallic Te.

All the films that exhibited a crystalline structure were subjected to Rietveld analysis to accurately determine the lattice parameters for each observed phase. To simulate XRD patterns, the following crystalline structures were used: trigonal Te (ISCD Card No. 96502; space group $P3_12_1$; unit cell parameters: a = b = 4.458 Å, c = 5.925 Å), orthorhombic γ-TeO_2 phase (ISCD Card No. 90733; space group $P2_12_12_1$; unit cell parameters: a = 4.898 Å, b =

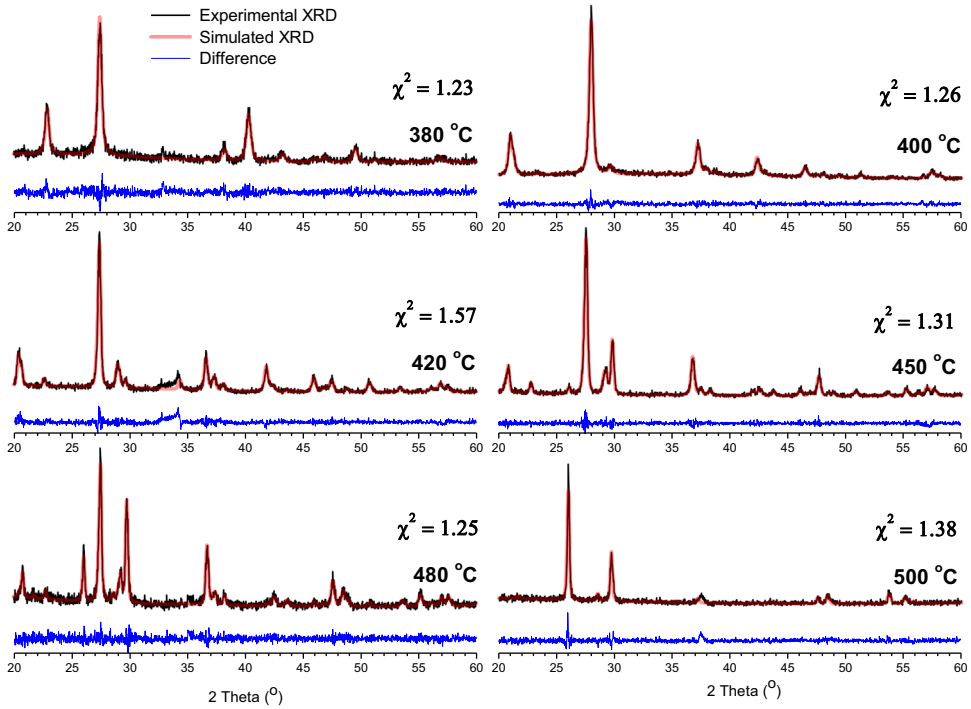

Fig. 3 Rietveld output plot of the investigated thin films, showing the observed (black) and calculated (orange) intensities and the difference between them (blue)

Table 1 Parameters obtained from the Rietveld refinement of the investigated thin films

	Lattice Parameters (Å)									Weight fraction (%)		
T (°C)	Te			γ-TeO_2			α-TeO_2			Te	γ-TeO_2	α-TeO_2
380	$a = 4.469$	$b = 4.469$	$c = 5.914$							100	0	0
	$\alpha = 90$	$\beta = 90$	$\gamma = 120$									
400				$a = 4.875$	$b = 8.606$	$c = 4.321$				0	100	0
				$\alpha = 90$	$\beta = 90$	$\gamma = 90$						
420				$a = 4.877$	$b = 8.592$	$c = 4.359$	$a = 4.834$	$b = 4.834$	$c = 7.606$	0	94.4	5.6
				$\alpha = 90$	$\beta = 90$	$\gamma = 90$	$\alpha = 90$	$\beta = 90$	$\gamma = 90$			
450				$a = 4.876$	$b = 8.596$	$c = 4.350$	$a = 4.811$	$b = 4.811$	$c = 7.612$	0	81.9	18.1
				$\alpha = 90$	$\beta = 90$	$\gamma = 90$	$\alpha = 90$	$\beta = 90$	$\gamma = 90$			
480				$a = 4.875$	$b = 8.599$	$c = 4.350$	$a = 4.810$	$b = 4.810$	$c = 7.620$	0	59.5	40.5
				$\alpha = 90$	$\beta = 90$	$\gamma = 90$	$\alpha = 90$	$\beta = 90$	$\gamma = 90$			
500							$a = 4.811$	$b = 4.811$	$c = 7.620$	0	0	100
							$\alpha = 90$	$\beta = 90$	$\gamma = 90$			

8.576 Å, c = 4.351 Å), and tetragonal α-TeO_2 phase (ISCD Card No. 161691; space group $P4_12_12$; unit cell parameters: a = b = 4.810 Å, c = 7.621 Å). Figure 3 shows the Rietveld output plot of the analyzed thin films, and the structural parameters extracted from the refinement are summarized in Table 1. All the goodness of fit (χ^2) values obtained were close to 1, indicating the reliability of the Rietveld refinement. All the calculated values of the lattice parameters well fit those of the crystalline structures used for refinement.

The XRD patterns of the film heat treated at 380 °C well coincided ($\chi^2 = 1.23$) with the trigonal crystalline phase of the metallic Te. On the other hand, the XRD pattern of the film treated at 400 °C was fitted only with the γ-TeO_2 orthorhombic phase ($\chi^2 = 1.26$). The treatments above 400 °C allowed the observation of the progressive transformation of γ-TeO_2 into the α-TeO_2 phase. The refinement clearly showed the coexistence of the orthorhombic γ-TeO_2 and tetragonal α-TeO_2 phases in the films treated at 420 °C, 450 °C, and 480 °C. The major contribution is related to the γ-TeO_2 phase, with 94.4%, 81.9%, and 59.5% weight fractions in the films treated, respectively, at 420 °C, 450 °C, and 480 °C. Moreover, the Rietveld refinement indicated the existence of only the tetragonal α-TeO_2 phase in the thin film treated at 500 °C.

The refinement showed the texture feature in all the films, but more strongly in the thin films that exhibited the γ-TeO_2 phase. The γ-TeO_2 crystalline phase (metastable) had a higher preferential growth trend than the α-TeO_2 stable phase. For example, the texture index of the γ-TeO_2 phase was 371 times higher than that of the α-TeO_2 phase in the film treated at 480 °C, in which the contribution of each phase was practically the same.

Table 2 presents the values of the crystallite size and strain of each TeO_2 phase observed in the investigated films, which were evaluated using the Williamson-Hall method. The FWHM values of the diffraction peaks were obtained from the simulated histogram of each existing phase. For the film treated at 420 °C, it was possible to determine these parameters only for the gamma phase because the contribution of the alpha phase was very small (5.6%).

Table 2 Average crystallite size and strain of the γ- and α-TeO_2 phases observed in the thin films treated at different temperatures

Thin Film treated at	Crystallite Size (nm)		Strain (10^{-3})	
(°C)	γ-TeO_2	α-TeO_2	γ-TeO_2	α-TeO_2
400	27 ± 2		2.1 ± 0.2	
420	53 ± 3		2.7 ± 0.1	
450	50 ± 3	67 ± 4	2.4 ± 0.1	2.6 ± 0.1
480	44 ± 1	68 ± 2	1.38 ± 0.05	2.17 ± 0.04
500		62 ± 2		1.80 ± 0.05

The values and respective errors were determined by plotting β *hklcos*θ vs *sin*θ for each diffraction peak (at least three were used). The linear fit of the plotted points provides the value and standard deviation of the slope and intercept of the straight line obtained. The slope provides the strain and the intercept the average crystallite size, according to eq. [1]

Heat treatment at 400 °C favored the nucleation and formation of the γ-TeO_2 crystalline phase. As expected, the heat treatments above this temperature favored the increase in the crystallite size of this crystalline phase, in addition to favoring the nucleation and formation of the α-TeO_2 crystalline phase. The coexistence of the two phases in the films caused an increase in the films' strains, and as expected, the values decreased with the increase of the treatment temperature.

Figure 4 shows the Raman spectra of the TeO_2 thin films treated at 350 °C, 400 °C, 450 °C, and 500 °C. In the film treated at 350 °C, only a single narrow peak at 522 cm^{-1}

was observed, which is attributed to the crystalline Si (substrate) [30].

The spectra of the films treated at 400 °C and 450 °C showed bands associated with the γ-TeO2 phase located at 819, 683, 612, and 424 cm^{-1} [31–33]. On the other hand, the spectrum of the film treated at 500 °C showed only bands associated with the α-TeO2 phase located at 648, 592, and 393 cm^{-1}. The pairs of strong and weak bands located at 683 and 612 cm^{-1}, respectively, in the γ-TeO_2 phase and at 648 and 592 cm^{-1} in the α-TeO2 phase are of the same nature [32]. These pairs of bands, strong and weak, are attributed to the symmetrical and asymmetric stretching modes, respectively, of the Te-O_{eq} bonds. These pairs of bands are spaced 71 cm^{-1} in the γ-TeO2 phase and 56 cm^{-1} in the α-TeO2 phase (Fig. 5), in agreement with those observed in the spectra obtained from the TeO_2 powder [32–35].

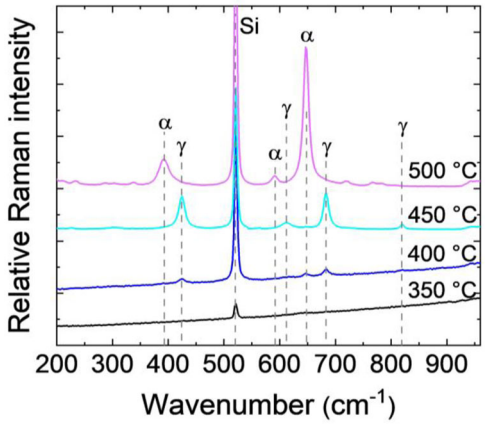

Fig. 4 Raman spectra of the TeO2 thin films treated at different temperatures

The two vibrational bands observed at 819 (weak) and 424 cm^{-1} (strong) in the spectrum of the film treated at 400 °C indicate that the structure of the γ-TeO_2 phase is different from the structure of the α-TeO_2 phase. There are two types of Te-O-Te bridge in the γ phase structure [32]: (1) a highly asymmetric bridge (Te-O···Te), similar to those observed in the α- and β-TeO_2 phases, where the shortest Te-O_{eq} bond is alternated with a much longer Te···O axial contact; and (2) a much more symmetrical bridge (Te-O-Te), where the distances between the Te-O bonds of the

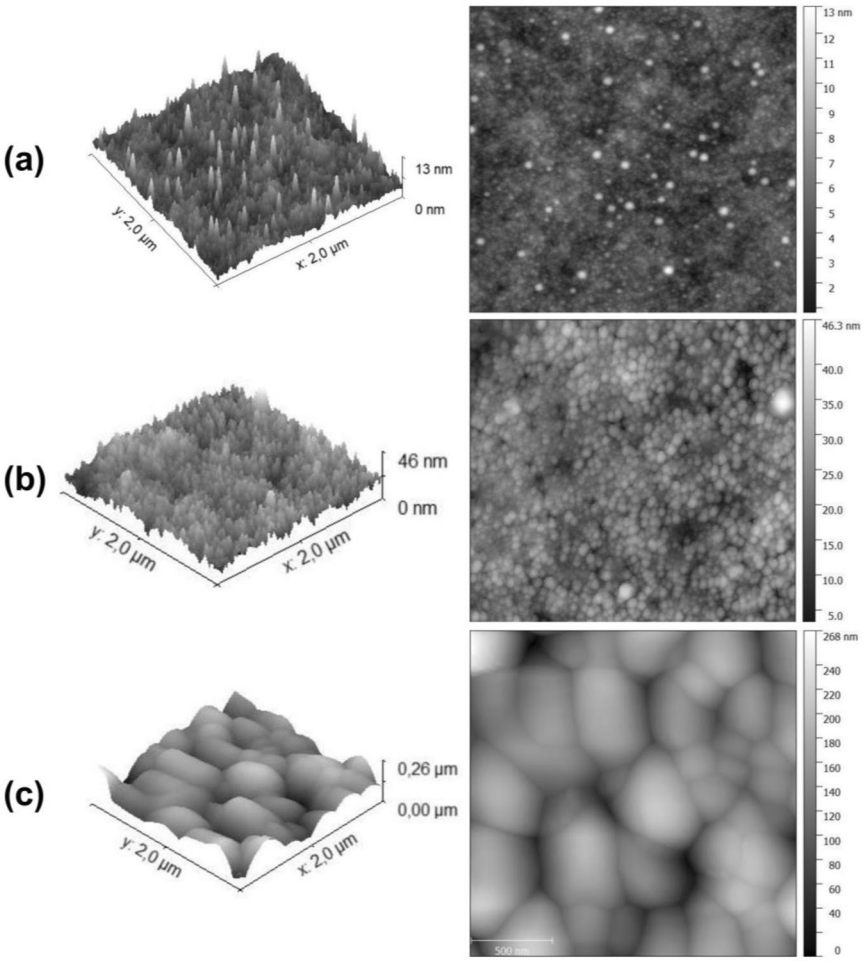

Fig. 5 AFM surface morphologies of the (**a**) as-prepared TeO_2 thin film, (**b**) the film heat treated at 400 °C, and (**c**) the film heat treated at 500 °C

bridge are very short. Consequently, a strong (symmetrical) band at 424 cm^{-1} and a very weak (asymmetric) band at 819 cm^{-1} were observed. Finally, the vibrational band located at 393 cm^{-1}, observed in the spectrum of the film treated at 500 °C, is attributed to the bending mode of the TeO_2 molecule [31].

Two-dimensional and three-dimensional (3D) AFM images of the TeO_2 thin films before heat treatment (as-prepared) and after heat treatment at 400 °C and 500 °C are presented in Fig. 5, which shows the films' surface morphologies.

The as-prepared film (Fig. 5a) exhibited a very homogeneous morphology with a small root mean square surface roughness of 1.01 nm, which was evaluated from a 2×2 µm image. The pores (dark pinholes) that emerged during the structural formation of the film could be observed. The heat treatment in the films caused an increase in the surface roughness (to 5.1 and 38.6 nm in the films treated at 400 °C and 500 °C, respectively). This increase in roughness was accompanied by an increase in grain size. Furthermore, Fig. 5b, c shows expressive grain growth during the transformation of γ- TeO_2 into α-TeO_2. The increase in crystallite size and decrease in strain, which had previously been observed in the XRD data (Table 2), accompanied with grain growth indicate defects reduction in crystalline structure.

The 3D micrographs showed the presence of hills and valleys on the surfaces of the films. The sharpness and the number of hills increased, however, with the heat treatment of the films. By comparing the surfaces of the as-prepared film and the film treated at 400 °C, it was possible to observe the growth of the columnar structure on the surfaces of the films due to the nucleation and grain growth during the crystallization process. After the heat treatment at 500 °C, the γ- TeO_2 transform to α-TeO_2 phase and the hill height and grain size increased, causing a decrease in the number of grains per area. At high temperatures, atoms acquire enough energy to move and occupy the correct site in the crystal lattice, and grains with lower surface energy will become larger [36, 37]. The image shows the coalescence of grains in the film structure, justifying the observed increase in grain size, and consequently, in the surface roughness.

4 Conclusions

Excellent-quality TeO_2 thin films were obtained using a simple and low-cost method. A precursor solution was prepared through the Pechini method using telluric acid, citric acid, and ethylene glycol as precursors. The films were deposited on Si substrates via spin coating.

An amorphous TeO_2 film was obtained after heat treatment at 350 °C for 2 h. Crystalline TeO_2 films containing only the γ- or α-TeO_2 phase were obtained after heat treatment, respectively, at 420–450 °C or 500 °C, both for 2 h. With the heat treatment of the thin films at 380–500 °C for 2 h, it was possible to observe: the formation of TeO_2 from metallic Te; the transformation of the TeO_2 phases from γ- (metastable phase) to α-TeO_2 (stable phase); and the influence of the heat treatment temperature on the crystallite size and the surface roughness of the thin film.

Author contributions Study conception and design were proposed by JCSM, MDB, and FBC. Material preparation and data collection were performed by MDB. The analysis were carried out by all authors. The first draft of the manuscript was written by MDB and all authors commented on previous versions of the manuscript. All authors read and approved the final manuscript.

Funding This work was supported by the Coordenação de Aperfeiçoamento de Pessoal de Nível Superior (Finance Code 001), Conselho Nacional de Desenvolvimento Científico e Tecnológico (CNPq) (Finance Code 307869/2015-6), and Fundação de Amparo à Pesquisa do Estado de São (Finance Code 17/13769-1).

Compliance with ethical standards

Conflict of interest The authors declare no competing interests.

References

1. Tirupataiah C, Narendrudua T, Suresh S, Rao PS, Vinaya Teja PM, Sambasiva Rao MV, Chinna Ram G, Krishna Rao D (2017) Influence of valence state of copper ions on structural and spectroscopic properties of multi-component PbO-Al_2O_3-TeO_2-GeO_2-SiO_2 glass ceramic system—a possible material for memory switching devices. Opt Mater 73:7–15. https://doi.org/10.1016/j.optmat.2017.07.040
2. Chen H, Liu YH, Zhou YF, Jiang ZH (2005) Spectroscopic properties of Er^{3+}-doped tellurite glass for 1.55 µm optical amplifier. J Alloy Compd 397:286–290. https://doi.org/10.1016/j.jallcom.2004.12.051
3. Anashkina EA (2020) Laser sources based on rare-earth ion-doped tellurite glass fibers and microspheres. Fibers 8:30. https://doi.org/10.3390/fib8050030
4. Yang K, Xu R, Meng Q, Chen L, Zhao S, Shen Y, Xu S (2008) Er^{3+}/Yb^{3+} co-doped TeO_2–ZnO–ZnF_2–La_2O_3 glass with a high fluorescence intensity ratio for an all-fiber temperature sensor. J Lumin 222:117145. https://doi.org/10.1016/j.jlumin.2020.117145
5. Dewan N, Sreenivas K, Gupta V (2008) Comparative study on TeO_2 and TeO_3 thin film for γ-ray sensor application. Sens Actuators, A 147:115–120. https://doi.org/10.1016/j.sna.2008.04.011
6. Arafat MM, Dinan B, Akbar SA, Haseen ASMA (2012) Gas sensor based on one dimensional nanostructured metal-oxides: a review. Sens (Basel) 12:7207–7258. https://doi.org/10.3390/s120607207
7. Yousef E, Hotzel M, Russel C (2004) Linear and non-linear refractive indices of tellurite glasses in the system TeO_2–WO_3–ZnF. J Non-Cryst Solids 342:82–88. https://doi.org/10.1016/j.jnoncrysol.2004.07.003
8. Wang JS, Vogel EM, Snitzer E (1994) Tellurite glass: a new candidate for fiber devices. Opt Mater 3:187–203. https://doi.org/10.1016/0925-3467(94)90004-3

9. Porter Y, Ok KM, Bhuvanesh NSP, Shuv Halasyamani P (2001) Synthesis and characterization of Te_2SeO_7: A powder second-harmonic-generation study of TeO_2, Te_2SeO_7, Te_2O_5, and $TeSeO_4$. Chem Mater 13:1910–1915. https://doi.org/10.1021/cm001414u
10. Vrillet G, Lasbrugnas C, Thomas P et al. (2006) Efficient second harmonic generation in γ-TeO_2 phase. J Mater Sci 41:305–307. https://doi.org/10.1007/s10853-005-5183-6
11. Lecomte A, Bamière F, Coste S, Thomas P, Champarnaud-Mesjard JC (2007) Sol-gel processing of TeO_2 thin films from citric acid stabilized tellurium isopropoxide precursor. J Eur Ceram Soc 27:1151–1158. https://doi.org/10.1016/j.jeurceramsoc.2006.05.029
12. Hodgson SNB, Weng L (2000) Preparation of tellurite thin films from tellurium isopropoxide precursor by sol-gel processing. J Non-Cryst Solids 276:195–200. https://doi.org/10.1016/S0022-3093(00)00254-4
13. Schartner EP, Monro TM (2014) Fiber tip sensor for localised temperature sensing based on Rare Earth-doped glass coatings. Sensors 14:21693–21701. https://doi.org/10.3390/s141121693
14. Sudha A, Maity TK, Sharma SL, Gupta AN (2018) An extensive study on the structural evolution and gamma radiation stability of TeO2 thin films. Mater Sci Semicond Process 74:347–351. https://doi.org/10.1016/j.mssp.2017.10.018
15. Siciliano T, Di Giulio M, Tepore M, Filippo E, Micocci G, Tepore A (2009) Room temperature NO_2 sensing properties of reactively sputtered TeO_2 thin films. Sens Actuators B Chem 137:644–648. https://doi.org/10.1016/j.snb.2008.12.004
16. Rashkova V, Kitova S, Vitanov T (2007) Electrocatalytic behavior of thin Co–Te–O films in oxygen evolution and reduction reactions. Electrochim Acta 52:3794–3803. https://doi.org/10.1016/j.electacta.2006.10.054
17. Munoz-Martin D, Fernandez H, Fernandez-Navarro JM, Gonzalo J, Solis J, Fierro JLG, Domingo C, Garcia-Ramos JV (2008) Nonlinear optical susceptibility of multicomponent tellurite thin-film glasses. J Appl Phys 104:113510–113515. https://doi.org/10.1063/1.3021052
18. Weng L, Hodgson SNB, Ma J (1999) Preparation of TeO_2-TiO_2 thin films by sol-gel process. J Mater Sci Lett 18:2037–2039. https://doi.org/10.1023/A:1006710606049
19. Ikeda H, Fujino S, Kajiwara T (2009) Preparation and characterization of BaO-TeO_2 thin films obtained from tellurium (VI) alkoxide by a sol-gel method. J Am Ceram Soc 92:2619–2622. https://doi.org/10.1111/j.1551-2916.2009.03280.x
20. Kumar A, Yadav N, Bhatt M, Mishra NK, Chaudhary P, Singh R (2015) Sol-gel-derived nanomaterials and its applications: a review. Res J Chem Sci 5:98–105. ISSN 2231-606X
21. Weng L, Hodgson S, Bao X, Sagoe-Crentsil K (2004) Achieving controllable sol-gel processing of tellurite glasses through the use of Te(VI) precursors. Mater Sci Eng B-Adv 107:89–93. https://doi.org/10.1016/j.mseb.2003.10.016
22. Mccusker LB, Von Dreele RB, Cox DE, Louer D, Scardi P (1999) Rietveld refinement guidelines. J Apl Crustallogr 32:36–50. https://doi.org/10.1107/S0021889898009856
23. Larson AC, Von Dreele RB (2000) General structure analysis system (GSAS), Los Alamos National Laboratory Report LAUR 86-748
24. Toby BH (2001) EXPGUI, a graphical user interface for GSAS. J Appl Crystallogr 34:210–213. https://doi.org/10.1107/S0021889801002242
25. Inorganic Crystal Structure Database. https://icsd.products.fiz-karlsruhe.de/en (accessed 13 October 2020)
26. Williamson GK, Hall WH (1953) X-ray line broadening from filed aluminium and wolfram. Acta Met Mater 1:22–31. https://doi.org/10.1016/0001-6160(53)90006-6
27. Rodrigues TS, Zhao M, Hang TH, Gilroy KD, Silva AGM, Camargo PHC, Xia Y (2018) Synthesis of colloidal metal nanocrystals: a comprehensive review on the reductants. Chem Eur J 24:16944–16963. https://doi.org/10.1002/chem.201802194
28. Lee H, Hong M, Bae S, Lee H, Park E, Kim K (2003) A novel approach to preparing nano-size Co_3O_4-coated Ni powder by the Pechini method for MCFC cathodes. J Mater Chem 13:2626–2632.9. https://doi.org/10.1039/b303980c
29. Barbooti MM, Al-Sammerrai DA (1986) Thermal decomposition of citric acid. Thermochim Acta 98:119–126. https://doi.org/10.1016/0040-6031(86)87081-2
30. Seo YH, Lee HJ, Jeon HI, Oh DH, Nahm KS, Lee YH, Suh EK, Lee HJ (1993) Photoluminescence, Raman scattering, and infrared absorption studies of porous silicon. Appl Phys Lett 62:1812–1814. https://doi.org/10.1063/1.109557
31. Ceriotti M, Pietrucci F, Bernasconi M (2006) Ab initio study of the vibrational properties of crystalline TeO_2: the α, β, and γ phases. Phys Rev B Condens Matter 73:104304. https://doi.org/10.1103/PhysRevB.73.104304
32. Mirgorodsky AP, Merle-Méjean T, Champarnaud JC, Thomas P, Frit B (2000) Dynamics and structure of TeO_2 polymorphs: model treatment of paratellurite and tellurite; Raman scattering evidence for new γ- and δ-phases. J Phys Chem Solids 61:501–509. https://doi.org/10.1016/S0022-3697(99)00263-2
33. Champarnaud-Mesjard JC, Blanchandin S, Thomas P, Mirgorodsky A, Merle-Méjean T, Frit B (2000) Crystal structure, Raman spectrum and lattice dynamics of a new metastable form of tellurium dioxide: γ-TeO_2. J Phys Chem Solids 61:1499–1507. https://doi.org/10.1016/S0022-3697(00)00012-3
34. Abu Sal B, Moiseyenko V, Dergachov M, Yevchik A, Dovbeshko G (2013) Manifestation of metastable γ-TeO_2 phase in the Raman spectrum of crystals grown in synthetic opal pores. Ukr J Phys Opt 14:119–124. https://doi.org/10.3116/16091833/14/3/119/2013
35. Dewan N, Sreenivas K, Gupta V (2007) Properties of crystalline gamma-TeO_2 thin film. J Cryst Growth 305:237–241. https://doi.org/10.1016/j.jcrysgro.2007.03.054
36. Lin Y, Xie J, Li Y, Chavez C, Lee S, Foltyn SR, Crooker SA, Burrell AK, McCleskey TM, Jia QX (2005) Green luminescent zinc oxide films prepared by polymer-assisted deposition with rapid thermal process. Thin Solid Films 492:101–104. https://doi.org/10.1016/j.tsf.2005.06.060
37. Fang ZB, Yan ZJ, Tan YS, Liu XQ, Wang YU (2005) Influence of post-annealing treatment on the structure properties of ZnO films. Appl Surf Sci 241:303–308. https://doi.org/10.1016/j.apsusc.2004.07.056